Perpendicular Magnetic Anisotropy and Spin Glass-like Behavior in Molecular Beam Epitaxy Grown Chromium Telluride Thin Films

Anupam Roy,* Samaresh Guchhait, Rik Dey, Tanmoy Pramanik, Cheng-Chih Hsieh, Amritesh Rai, and Sanjay K Banerjee

Microelectronics Research Center, The University of Texas at Austin, Austin, Texas 78758, United States

ABSTRACT Reflection high-energy electron diffraction (RHEED), scanning tunneling microscopy (STM), vibrating sample magnetometry, and other physical property measurements are used to investigate the structure, morphology, magnetic, and magnetotransport properties of (001)-oriented Cr_2Te_3 thin films grown on Al_2O_3(0001) and Si(111)-(7×7) surfaces by molecular beam epitaxy. Streaky RHEED patterns indicate flat smooth film growth on both substrates. STM studies show the hexagonal arrangements of surface atoms. Determination of the lattice parameter from the atomically resolved STM image is consistent with the bulk crystal structures. Magnetic measurements show the film is ferromagnetic, having a Curie temperature of about 180 K, and a spin glass-like behavior was observed below 35 K. Magnetotransport measurements show the metallic nature of the film with a perpendicular magnetic anisotropy along the *c*-axis.

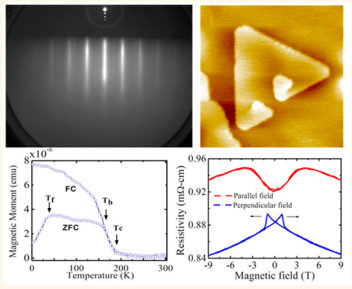

KEYWORDS: chromium telluride · molecular beam epitaxy · scanning tunneling microscopy · ferromagnetic metal · spin glass · magnetoresistance · perpendicular magnetic anisotropy

Transition-metal chalcogenides have attracted much interest in the past due to their large variety of novel physical, electrical, and magnetic properties. On the one hand, these can be metallic, half-metallic, or semiconducting depending on the anion and on the ratio between the transition metal and chalcogen atoms. On the other hand, these chalcogenides may have ferromagnetic, antiferromagnetic, or noncollinear spin structure for different crystal structures and compositions. The chromium−tellurium system has a large family of compounds. There are various stable stoichiometries [*e.g.*, $Cr_{1-x}Te$, Cr_2Te_3, Cr_3Te_4, Cr_5Te_8] depending on the Cr vacancies that occur in every second metal layer. Thus, Cr-deficient and Cr-full layers stack alternately along the *c*-axis.[1] All of these chromium chalcogenides have NiAs-type crystal structures, and the stable phases are ferromagnetic, with a wide range of Curie temperatures, T_c, between 180 to 340 K. T_c depends very sensitively on the composition of the compound. Wontcheu *et al.*[1] have shown the effect of anion substitution on the structural and magnetic properties of chromium chalcogenides. The physical properties change drastically with the change in composition.

Because of its unusual magnetic properties, Cr_2Te_3 is one of the interesting compounds in this family. Recently, Akiyama *et al.* have used a thin Cr_2Te_3 ferromagnetic metallic film in a field-effect capacitor (FEC) structure.[2] Saito *et al.* have studied tunneling magnetoresistance (TMR) in the magnetic tunneling junctions (MTJs) with $Cr_{1-\delta}Te$ being one of the electrodes.[3] Several groups have studied the electronic and magnetic structures of Cr_2Te_3 bulk samples theoretically[4,5] as well as experimentally.[1,6−11] There are only a few reports of the epitaxial growth of $Cr_{1-\delta}Te$ thin films on GaAs(001) substrates.[2,12−15] However, a detailed study of the structure and magnetic and transport properties of Cr_2Te_3 thin films is lacking. We have studied the growth of Cr_2Te_3 thin films directly on Si(111)-(7×7) and Al_2O_3(0001) surfaces using molecular beam epitaxy (MBE).

* Address correspondence to anupam@austin.utexas.edu.

Received for review November 18, 2014 and accepted April 7, 2015.

Published online April 07, 2015
10.1021/nn5065716

We show the atomically resolved scanning tunneling microscopy (STM) micrographs of Cr_2Te_3 grown on Si(111)-(7×7) surfaces. Magnetic studies confirm the film to be ferromagnetic, with a spin glass-like behavior at low temperature. We also have observed the anisotropic magnetoresistance (AMR) on the grown film. AMR is a well-known phenomenon observed in ferromagnetic materials with metallic conductance where the resistance changes with the angle between the current flow direction and the magnetization direction.[16] Interestingly, the grown films possess perpendicular magnetic anisotropy (PMA). Ferromagnetic PMA thin films have attracted interest due to their interesting fundamental properties and technological applications in magnetic recording,[17,18] MTJs,[19] and spin-transfer torque (STT) devices.[20,21] Details of growth, structural, magnetic, and transport properties are presented in the paper.

RESULTS AND DISCUSSION

Growth and Structural Properties. Previous reports were on the growth of $Cr_{1-\delta}Te$ using MBE on GaAs(001) substrates with buffer layers of ZnTe and CdTe.[2,12−15] Here, we present the MBE growth of Cr_2Te_3 thin film of different thicknesses directly on UHV-cleaned Al_2O_3(0001) and Si(111)-(7×7) substrates without any additional buffer layer. An *in situ* reflection high-energy electron diffraction (RHEED) study, monitored during the MBE growth of Cr_2Te_3 films grown on Al_2O_3(0001) and Si(111)-(7×7) substrates, is shown in Figure 1. Figure 1a and b show the RHEED patterns from a clean Al_2O_3(0001) substrate surface along the $[1\ 0\ -1\ 0]_{Al2O3}$ and $[1\ 1\ -2\ 0]_{Al2O3}$ electron beam incidence, respectively. Corresponding RHEED patterns from the same surface following growth of Cr_2Te_3 thin films are shown in Figure 1c and d. Similar smooth film growth has also been achieved on Si(111) substrates. RHEED patterns of a reconstructed Si(111)-(7×7) surface are shown in Figure 1e for the electron beam along the $[1\ 1\ -2]_{Si}$ direction and in Figure 1f for $[1\ -1\ 0]_{Si}$ incidence. Corresponding RHEED patterns from a Cr_2Te_3 film show sharp streaky features in Figure 1g and h. This is evidence that, on both the substrates, Cr_2Te_3 grows with a high crystalline quality, giving atomically flat surface morphologies. Several samples with different thicknesses prepared on both the substrates show similar RHEED patterns, and the RHEED patterns were maintained throughout the entire growth process. The growth is along the (001) direction (also evident from XRD), which is very consistent for the growth of a hexagonal thin film on hcp(0001) or fcc(111) substrates. Similar (001)-oriented hexagonal thin film growth on an fcc(111) structure has also been reported for Bi_2Te_3(0001) on Si(111) surfaces.[22]

Figure 2a shows the X-ray diffraction (XRD) pattern from a 12 nm thin film of Cr_2Te_3 grown on an Al_2O_3(0001) substrate. The diffraction pattern matches

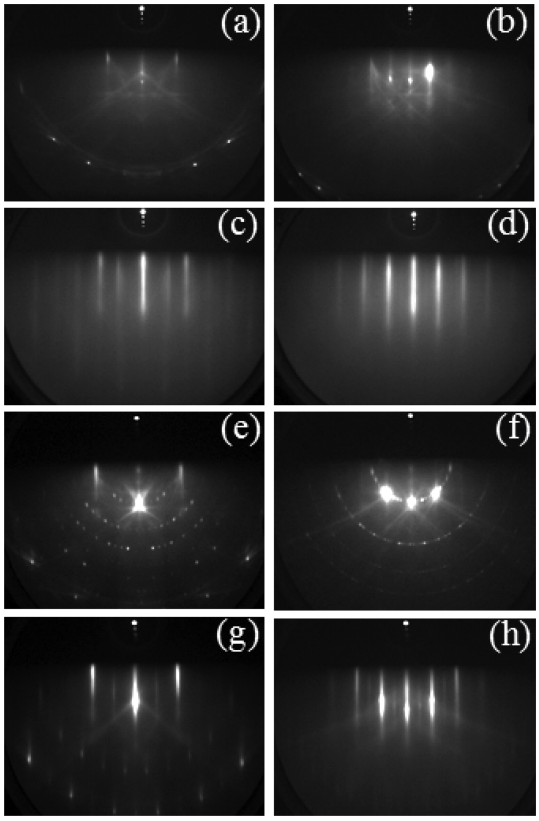

Figure 1. RHEED images following Cr_2Te_3 growth on Al_2O_3(0001) and Si(111)-(7×7) surfaces. (a and b) RHEED patterns from a clean Al_2O_3(0001) surface with the incident electron beam along the [1 0 −1 0] and [1 1 −2 0] orientations of Al_2O_3, respectively. (c and d) Corresponding RHEED patterns from the same surface following 4 nm of Cr_2Te_3 growth. (e and f) Typical (7×7) surface reconstruction from a Si(111) substrate along the [1 1 −2] and [1 −1 0] orientations of Si, respectively. (g and h) Corresponding RHEED patterns following 8 nm of Cr_2Te_3 growth.

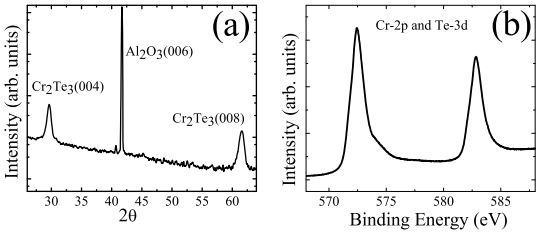

Figure 2. (a) XRD pattern from 12 nm of an epitaxial Cr_2Te_3 thin film. The pattern shows that the growth is along the (001) direction. (b) Cr-2p and Te-3d core-level X-ray photoelectron spectra from 12 nm of a Cr_2Te_3 thin film.

very well with the NiAs-type hexagonal structure with the $P\bar{3}1c$ (163) space group. Peaks from (004) and (008) planes of Cr_2Te_3 film are indexed in Figure 2a. It clearly shows that the grown film is following the underlying crystal symmetry of the substrate and growing along the (001) direction. The XRD pattern also rules out any significant presence of any impurities or other known phases of chromium telluride. *In situ* X-ray photoelectron spectroscopy (XPS) measurement from a 12 nm thick Cr_2Te_3 film grown on an Al_2O_3(0001)

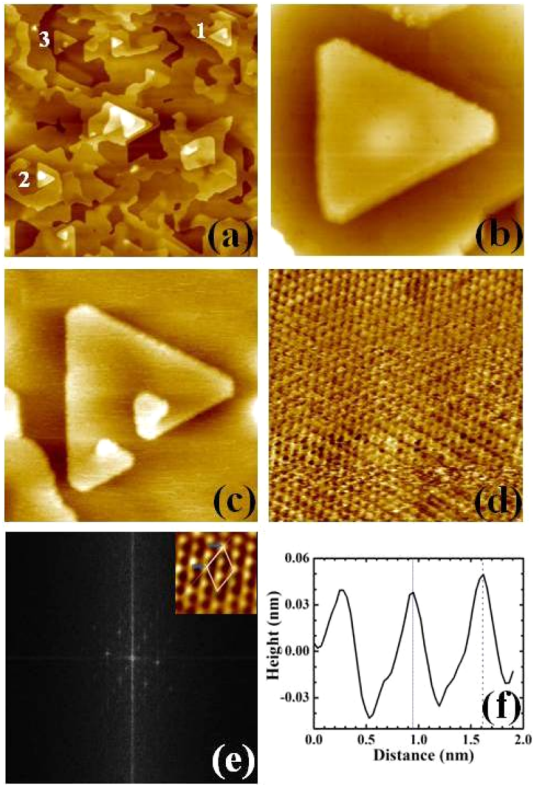

Figure 3. STM study of a 8 nm epitaxial Cr_2Te_3 thin film grown on Si(111)-(7×7) surfaces. (a) Several triangular features along with spirals having clockwise and anticlockwise rotations (scan area: 500 × 500 nm^2, bias voltage: −1 V, tunneling current: 0.2 nA). (b) Truncated hexagon structure indicating the influence of substrate surface symmetry (scan area: 60 × 60 nm^2, bias voltage: −1 V, tunneling current: 0.2 nA). (c) Two spirals of opposite sign on a truncated hexagon (scan area: 70 × 70 nm^2, bias voltage: −1 V, tunneling current: 0.2 nA). (d) Atomically resolved STM image showing hexagonal units on the surface (scan area: 10 × 10 nm^2, bias voltage: −1 V, tunneling current: 0.2 nA). (e) Fourier transformed pattern from the STM image in (d) showing diffraction spots corresponding to hexagonal unit cells. (Inset) FFT-filtered STM image showing hexagonal arrangement of surface atoms. One unit cell is marked. (f) Profile drawn across the line marked on the hexagonal unit in the inset of (e).

substrate shows the peaks corresponding to Cr and Te. Figure 2b shows Cr-2p and Te-3d peaks. Since the binding energies of these two peaks are very close to each other, it is difficult to separate them out. The positions of the peaks are consistent with the reported results.[23]

A detailed microscopy study of a Cr_2Te_3 thin film has been lacking, as previous studies do not present any high-resolution microscopy study. Sreenivasan *et al.*[14] have studied the roughness of the grown film by *ex situ* atomic force microscopy in a length scale that cannot reveal the surface structure at the atomic level. In Figure 3, we present an extensive *in situ* STM study of the surface of a Cr_2Te_3 thin film grown on Si(111)-(7×7) surfaces. As observed from Figure 3a, the structures are characteristically triangular shaped, reflecting the hexagonal crystal structure along the (001) direction. This is not surprising, as both hcp(0001) and fcc(111) surfaces have a hexagonal Bravais lattice and differ only in the registry of the third layer.[24] Because of the surface symmetry, the formation of equilateral triangles on the Si(111) substrate is quite natural. Triangle-shaped structures and terraces have also been observed for the growth of hexagonal Bi_2Se_3(0001) on Si(111) surfaces.[25,26] Formation of different shapes of structures, including triangular and hexagonal on a surface of 3-fold symmetry, has been shown by kinetic Monte Carlo simulation studies.[27,28] The hexagonal structures on fcc(111) surfaces can have two types of edges. The final shape of the grown structure is determined by the competition of the advancement rate of these two types of edges.[27,28] Careful investigation reveals that, in our case, structures are truncated triangular (or, more precisely, triangular hexagon) in shape (Figure 3b and c), as should be the case when one type of edge advances faster than the other edge. Similar triangular hexagon structures have also been observed for the growth of $CoSi_2$ on Si(111) surfaces.[29] STM measurements carried out on several Cr_2Te_3 thin films of different thicknesses (4 to 20 nm) show similar triangular hexagons and hexagonal surface lattices, indicating the growth follows strictly the underlying crystal symmetry.

Figure 3a also shows the spirals and depressions in the grown film. One such spiral on a triangular hexagon structure is shown in Figure 3c. Spiral growth mode is observed for crystals with atomically flat surfaces. Such crystals grow by adatom incorporation at monatomic steps. The spiral growth mode is very common for GaN growth on SiC(0001) and Al_2O_3(0001) substrates, where the origin of spiral growth has been determined to be high-density threading dislocations with a screw component.[30] Pioneering theoretical work by Burton, Cabrera, and Frank (BCF) shows that a screw dislocation emerging from a crystal provides a continuous step source on the surface leading to the formation of growth spirals.[31] During growth this step winds around the dislocation center and thus forms a spiral. For a Cr_2Te_3 thin film grown on Si(111) substrates, the spiral density is observed to be much lower compared to GaN growth. All the spirals observed are single-arm spirals only. Any cooperative spirals with more than one arm are absent. Cui *et al.*[30] discussed the formation and annihilation of several types of spirals and different interactions between them. A spiral will be stable if the curvature of the spiral is more than a critical value. These spirals can be rotating clockwise and counterclockwise. Figure 3a shows that both types of rotations are present in Cr_2Te_3 spirals. Two such spirals present on two different triangular structures are shown (marked as "1" and "2") to have opposite rotations. The structure marked as "3" contains two spirals of opposite sign on the same triangular structure. Figure 3c also shows one of such instances where two spirals are on the same truncated hexagon.

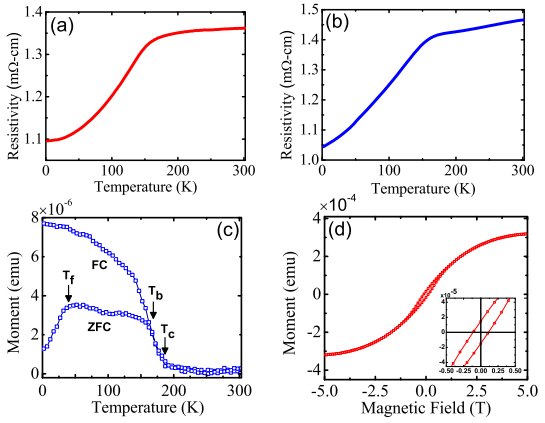

Figure 4. Temperature dependence of electrical resistivity showing metallic behavior. (a) 4 nm and (b) 20 nm epitaxial Cr_2Te_3 films grown on Al_2O_3(0001) and Si(111)-(7×7) substrate surfaces, respectively. Magnetic studies from a Cr_2Te_3 thin film grown on a Si(111)-(7×7) surface. (c) Zero-field-cooled (ZFC) and field-cooled (FC) magnetization as a function of temperature with a 500 Oe magnetic field along the surface plane. (d) Hysteresis loops of a Cr_2Te_3 thin film at 2 K with the magnetic field parallel to the surface plane showing nonsaturating magnetization even with a 5 T magnetic field. The inset shows an enlarged portion of the hysteresis loop around the origin.

Figure 3d shows the atomically resolved structure of the Cr_2Te_3 surface. A hexagonal lattice arrangement on the surface is observed at room temperature (RT). In Figure 3e, the fast Fourier transformed (FFT) pattern from the image in Figure 3d shows the periodic spots corresponding to the Cr_2Te_3 hexagonal surface symmetry. The inset shows the FFT-filtered STM image, clearly indicating the hexagonal arrangement of surface atoms. One such hexagonal unit cell is marked (inset). Line profile drawn along one side of the marked hexagonal unit (arrow marked) is shown in Figure 3f. The lattice parameter *a*, from the line profile (marked as two vertical lines), is determined to be 6.68 Å, which is very close to the corresponding bulk Cr_2Te_3 lattice parameter (6.81 Å) at RT as measured from the neutron diffraction study.[8] The lattice parameter obtained from the STM measurement also agrees very well with the measurement from the transmission electron diffraction study as shown in ref 12.

Transport and Magnetic Properties. Figure 4a and b show the electrical resistivity measured from 300 K down to 2 K. The measurements were conducted using standard van der Pauw geometry on a Cr_2Te_3 thin film grown on Al_2O_3(0001) and Si(111) substrates of thicknesses 4 and 20 nm, respectively. Both the curves show metallic behavior for the entire temperature range. The slopes of the electrical resistivity curves change abruptly at ~180 K, which corresponds to the magnetic phase transition temperature. Magnetic measurement (Figure 4c) also shows that the Curie temperature (T_c) of the film is ~180 K. Below the Curie temperature, the electrical resistivity decreases more rapidly with temperature than above the Curie temperature. This may be because of reduction in electron−magnon scattering due to ferromagnetic spin alignment, which is explained next. The electrical resistivity curve for $Cr_{1.96}Te_3$ bulk samples also shows a transition point around a similar temperature range.[10] A similar trend in resistivity is also observed for ferromagnetic transition metals, where the resistivity of a ferromagnetic metal can be described as $\rho(T) = \rho_0 + \rho_L(T) + \rho_M(T)$. Here ρ_0 is the residual resistivity at absolute zero arising due to the scattering of electrons from lattice defects and impurities, and $\rho_L(T)$ comes from the scattering of conduction electrons by the lattice vibrations (phonons), which increases with temperature. The additional $\rho_M(T)$ term arises only for the ferromagnetic materials as the electrons get scattered by magnons below T_c.[32] The magnetic scattering arises from the s−d exchange interaction between the conduction electrons and the more localized 3d magnetic electrons.[33] Above T_c, the spins are disordered and the resistance due to scattering related to magnetic order approaches a temperature-independent saturation value. However, below T_c, spontaneous magnetization appears, which aligns spins along the magnetization direction. Ferromagnetic alignment of spins reduces the electron−magnon scattering. When the temperature is lowered, more spins align ferromagnetically (Figure 4c), and this leads to further reduction of electron−magnon scattering with decreasing temperature. Careful observation also reveals that the percentage change of resistance below T_c is lower than that observed in typical transition metals.[34] This is probably due to the presence of magnetic domains and their freeze out in random direction with decreasing temperature. Electrons get scattered at domain boundaries, and hence the reduction of resistance is smaller than a bulk, uniformly magnetized sample.

Magnetic measurements from a 20 nm Cr_2Te_3 film grown on Si(111) surfaces have been shown in Figure 4c and d. Figure 4c shows the variation of the field-cooled (FC) and zero-field-cooled (ZFC) magnetization with temperature in a magnetic field of 500 Oe along the surface plane of a Cr_2Te_3 thin film. Field-cooled magnetization (M_{FC}) shows a paramagnetic-to-ferromagnetic transition at T_c = 180 K and increases continuously with decreasing temperature below T_c. A strong continuous increase of M_{FC} below T_c indicates the ferromagnetic nature of the grown film. The reported T_c for Cr_2Te_3 bulk samples (170−180 K) matches very well with our result.[4,10,11] The magnetic hysteresis curve at 2 K, shown in Figure 4d, also indicates the ferromagnetic nature of the film. The magnetic moment is determined to be ~2.8 μ_B per Cr atom (μ_B is the Bohr magneton). The itinerant nature of Cr 3d electrons appears to be the reason behind this discrepancy from the expected saturation magnetic moment of 3 μ_B per Cr atom calculated from an ionic model and also observed by others in bulk and thin film samples.[5,9,10,12]

The magnetization does not saturate completely even with a strong magnetic field (as observed in Figure 4d). This nonsaturation of magnetic moment has been observed for other transition-metal compounds where frustration is present and also has been reported before.[10,12] The existence of a spin glass phase in our sample (discussed below) also shows the presence of frustration in the Cr_2Te_3 sample.

Another interesting feature of Figure 4c is that the zero-field-cooled magnetization (M_{ZFC}) first increases and then becomes almost constant with increasing temperature. The temperature where this abrupt change of slope takes place is defined as the freezing temperature, T_f. On the contrary, M_{FC} always decreases with increasing temperature below T_c. Furthermore, with a further increase in temperature, M_{ZFC} first decreases slightly and then merges with M_{FC} at a temperature T_b just below T_c. Temperature T_b is also known as the blocking temperature. Above this temperature T_b, M_{ZFC} and M_{FC} superpose each other. The freezing temperature (T_f), an indication of a spin glass-like phase, is determined to be ~35 K. Also note that in Figure 4a and b a noticeable change in slope of the resistivity curves is observed near 35 K. However, a large difference between M_{FC} and M_{ZFC} values between T_f and T_b indicates the presence of short-range ferromagnetic ordering (*i.e.*, domains) within our sample. Freezing out of domains in random direction in the absence of any magnetic field can explain the observed difference between M_{FC} and M_{ZFC} magnetization curves,[35] as well as transport properties of our samples below T_c.

Spin glass-like behavior has also been reported for $Cr_7(Se_{1-x}Te_x)_8$ compounds before, resulting from the spin frustration due to the competition between the ferromagnetic and antiferromagnetic interactions.[1,36] Hui *et al.*[12] have suggested that antiferromagnetically coupled Cr^{3+} spins in the vacancy layer of a NiAs-type structure[4,12] may have a role in the observed intrinsic magnetic exchange bias in a structurally single-crystal Cr_2Te_3 film. As stated before, between T_c and T_f, M_{ZFC} is lower than M_{FC} due to the freeze out of the magnetic domains in random direction with decreasing temperature. However, we believe a spin glass-like phase appears below T_f that causes more randomization of magnetic moments within each domain, and hence M_{ZFC} drops more sharply with decreasing temperature.

Since with decreasing temperature here we have paramagnetic-to-ferromagnetic to spin glass transitions, we believe this might be a re-entrant-type spin glass phase. A re-entrant spin glass phase arises when both (stronger) ferromagnetic and (weaker) antiferromagnetic interactions are present within the same system. In such a situation, one will first see a ferromagnetic transition. However, for a "strong enough" antiferromagnetic interaction, the system becomes frustrated at lower temperatures, and hence

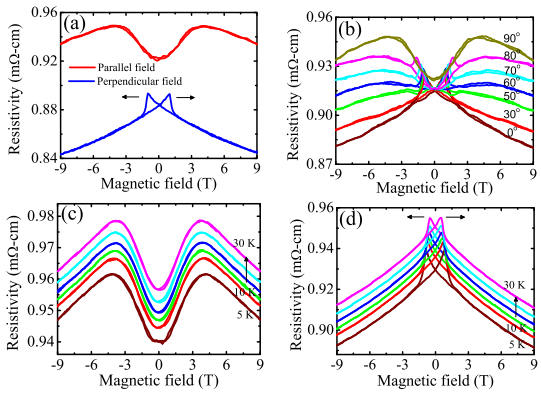

Figure 5. Variation of magnetoresistance (MR) at 2 K with the magnetic field applied parallel (θ = 90°) and perpendicular (θ = 0°) to the surface. (b) Variation of MR at 2 K with respect to the magnetic field at different orientations. Variation of MR with the magnetic field applied (c) parallel and (d) perpendicular to the surface at different temperatures.

a spin glass transition may happen at even lower temperature.[37] Hashimoto *et al.*[10] have claimed that both stronger ferromagnetic and weaker antiferromagnetic Cr−Cr interactions are present within Cr_2Te_3, and hence they have predicted the existence of more "complex magnetic order below the Curie temperature". We believe this may explain the origin of the re-entrant spin glass phase in our Cr_2Te_3 sample. Also note that the nonsaturation of the magnetic moment at a very large magnetic field at 2 K (Figure 4d) is a clear indication of frustrated interactions in this system. A similar coexistence of ferromagnetism and spin glass behavior has been observed in many systems, including amorphous Ge:Mn[38] and a cluster glass perovskite compound where the cusp in M_{ZFC} is governed by a local anisotropy field acting on the spins inside each domain.[39] This cluster glass phase is nothing but a modification to the spin glass system formed when the magnetic spin density is increased due to short-range ferromagnetic ordering, thus resulting in formation of magnetic clusters.[1,40,41] However, more studies are necessary to understand the true nature of the spin glass phase in Cr_2Te_3 and distinguish between different glassy systems (*e.g.*, cluster glass, reentrant spin glass, canted spin system) that can show many common macroscopic features.[40] This coexistence of ferromagnetism and re-entrant glassy behavior is an interesting new observation in Cr_2Te_3 thin films.

Figure 5a shows the variation of magnetoresistance (MR) at 2 K for the Cr_2Te_3 film grown on $Al_2O_3(0001)$ surfaces with the magnetic field oriented parallel (θ = 90°) and perpendicular (θ = 0°) to the surface plane. From parallel and perpendicular field MR, we conclude that the Cr_2Te_3 film possesses a perpendicular magnetic anisotropy, which is explained next. At zero-field value, the magnetic easy axis is normal to the surface and so is the magnetization direction. The resistance at zero field is minimum because the

magnetization direction is normal to the current flow direction. With a magnetic field applied parallel to the surface, the effective magnetization direction starts rotating toward the in-plane magnetic field until it saturates. At this saturation field (parallel to the surface), the magnetization reaches its saturation magnetization value, points toward the direction of current flow, and lies along the surface. Hence at this saturation field (~4 T at 2 K), the resistance also becomes maximum. This field dependence of MR corresponds to the anisotropic MR, which results from the anisotropy of the spin−orbit interaction in ferromagnetic materials.[16] For higher field values, the obtained MR is linear and shows negative slope, which is due to the suppression of weak localization (WL) and/or electron−electron interaction (EEI).[42−44] Hashimoto *et al.*[10] have studied the magnetization of Cr_2Te_3 bulk crystal and observed that the magnetic easy axis is pointing along the *c*-axis. As we have observed from RHEED, XRD, and the STM studies, Cr_2Te_3 grows epitaxially along the *c*-axis on Al_2O_3(0001) and Si(111) substrates. PMA observed from transport studies (Figure 5a) thus indicates a magnetic crystalline anisotropy present in the 4 nm thick Cr_2Te_3 epitaxial film.

When the magnetic field is applied perpendicular to the surface, the MR consists of two parts: one is almost linear, reversible negative MR at high field that arises due to the suppression of WL and/or EEI. In the smaller field range, MR shows a hysteresis with back-and-forth field sweep and has a sharp maximum. The two sharp maxima in the resistance correspond to the coercive field value (~1 T) where the domain wall density reaches its maximum (*i.e.*, the domains are all misaligned), and as a result, the resistance is also maximum due to increased scattering at domain boundaries. As the field increases, the domains start to align in the direction of the field and the resistance starts to decrease. However, this negative MR does not saturate even at high field (9 T) and low temperature (2 K), where most spins are ferromagnetically coupled with each other, due to suppression of WL and/or EEI. It is interesting to note that the resistance values at zero fields are not the same for parallel and perpendicular field sweeps. As the film possesses PMA, in a perpendicular field sweep more domains are aligned with each other at zero field, while in a parallel field sweep most domains are misaligned due to a previously applied parallel field. This causes the resistance value at zero field to be smaller for the perpendicular field sweep than that for the parallel field sweep.

The presence of PMA is also evident from the variation of MR with the magnetic field applied at different angles with respect to the surface normal (as shown in Figure 5b). Except for the parallel field sweep, the resistance values at zero field for the field sweeping in different orientations are almost the same. As long as there is some component of magnetic field in the perpendicular direction, the magnetization aligns along the easy axis of this PMA film and shows almost the same value of resistance at zero field. However, for the parallel field orientation, the magnetization does not align along the easy axis due to a previously applied parallel field and the resistance is higher at the zero field due to the maximum randomness in domain alignment. Also the magnetic field at which the peak appears in the MR increases with the change in field orientation from $\theta = 0°$ (perpendicular field) to $\theta = 90°$ (parallel field). As the field direction changes from perpendicular to parallel, a higher magnetic field is necessary to attain the maximum randomness. So it is clear that for a field oriented between 0° and 90° the MR is due to the competition between the components of magnetic field perpendicular and parallel to the surface. Figure 5c shows the parallel field MR at different temperatures. The saturation field value, where the slope of MR changes, decreases with increasing temperature, as expected for a ferromagnetic film. Figure 5d shows the perpendicular field MR at different temperatures. The coercive field value, where the sharp maximum in the MR occurs, decreases with increasing temperature, which is also a characteristic of a ferromagnetic film.[45] As the temperature increases, domains can more easily align along the applied field, and as a result the coercive field value is also smaller.

In several applications, materials with PMA are used for superior performances.[17−21] PMA is observed in very thin transition-metal layers, such as a 0.8 nm or less thick Co layer. Multilayers of transition metals with other nonmagnetic metals, such as Co/Pd multilayers, are used in MTJ-type devices. These types of PMA multilayers are used in MTJ because of higher thermal stability, more magnetic uniformity, and larger magnetic anisotropy energy compared to in-plane anisotropy materials. Moreover, for STT memory applications, PMA materials are useful due to the lower switching current requirement.[46] However, the presence of multi-interfaces increases the overall resistance of the film. A single-layer PMA film of Cr_2Te_3 can reduce the number of interfaces, thus reducing the overall loss of spin polarization due to inelastic scattering at the interfaces. Considering the saturation magnetization, M_S, of 620×10^3 A/m (from Figure 4d) and the anisotropy field, H_A, of 4.1 T (from Figure 5a), the PMA energy density, $E_p = -M_S H_A/2$, is estimated approximately to be 1.27×10^6 J/m^3. The estimated value is in reasonably good comparison with other PMA films.[47] As all the chromium telluride compounds are of the same NiAs-type crystal structure, one can expect to have a single-crystalline PMA film with a wide range of T_c for various Cr compositions. We believe this work opens up an opportunity to study the PMA property of chromium telluride films and provides an excellent possibility for various applications in a wide temperature range.

SUMMARY AND CONCLUSIONS

In conclusion, we have carried out the MBE growth of Cr_2Te_3 thin films on Al_2O_3(0001) and Si(111) substrates. Structural, magnetic, and transport properties of the films have been characterized by several *in situ* and *ex situ* techniques. Sharp streaks in RHEED patterns imply smooth thin film growth on both of the substrates. As observed from RHEED and XRD, the as-grown film is hexagonal and oriented along the (001) direction (*c*-axis). We have shown the hexagonal atomic arrangement of a Cr_2Te_3 film from high-resolution *in situ* STM measurements at room temperature. Magnetic measurement shows the film to be ferromagnetic, and a spin glass-like phase appears below 35 K. This shows competing interactions within Cr_2Te_3. Magnetotransport studies reveal that the film possesses perpendicular magnetic anisotropy in a 4 nm Cr_2Te_3 film, which has not been observed before. The presence of PMA makes it a very useful material for possible spintronics applications.

EXPERIMENTAL SECTION

Cr_2Te_3 films were grown in a custom-built MBE growth system (Omicron, Germany) under ultrahigh vacuum (UHV) conditions (base pressure $\sim 1 \times 10^{-10}$ mbar). Details of the system have been described elsewhere.[22] A RHEED setup is attached to the MBE system for *in situ* monitoring of surface reconstruction and growth. Substrates used in the experiment were insulating *c*-axis Al_2O_3(0001) and P-doped n-type Si(111) wafers (oriented within $\pm 0.5°$) with a resistivity of 1−20 Ω-cm. Atomically clean, reconstructed Si(111)-(7×7) surfaces were prepared by the usual heating and flashing procedure,[48] and *c*-Al_2O_3(0001) substrates were cleaned by the standard heating method in UHV. Clean substrate surfaces were examined by *in situ* RHEED. Chromium and tellurium fluxes generated by an e-beam evaporator and effusion cell, respectively, were co-deposited onto the substrates at an elevated substrate temperature of about 340 °C. The chamber pressure during growth never exceeded 1×10^{-9} mbar, and the Te_2/Cr BEP (beam equivalent pressure) flux ratio was kept at about 15. Several samples with thicknesses varying from 4 to 20 nm were grown, and the typical growth rate of Cr_2Te_3 films was about 0.1 nm/min.

Postgrowth investigations of the samples were carried out by *in situ* RHEED operated at 13 kV, STM at RT in the constant current mode, XPS with monochromatic Al Kα, and *ex situ* XRD. Magnetic and transport measurements were carried out with a 9 T Quantum Design physical property measurement system combined with vibrating sample magnetometry capable of cooling samples to ∼2 K.

Conflict of Interest: The authors declare no competing financial interest.

Acknowledgment. This work was supported by the NRI SWAN Center. We acknowledge helpful discussions with Prof. A. H. MacDonald, Prof. B. N. Dev, Dr. L. Colombo, Dr. Jiamin Xue, and Dr. Sumalay Roy. We also appreciate technical support from Omicron and Quantum Design.

REFERENCES AND NOTES

1. Wontcheu, J.; Bensch, W.; Mankovsky, S.; Polesya, S.; Ebert, H. Effect of Anion Substitution onto Structural and Magnetic Properties of Chromium Chalcogenides. *Prog. Solid State Chem.* **2009**, *37*, 226–242.
2. Akiyama, R.; Oikawa, H.; Yamawaki, K.; Kuroda, S. Electric-Field Modulation of Ferromagnetism in Hexagonal Chromium Telluride Thin Film. *Phys. Status Solidi C* **2014**, *11*, 1320–1323.
3. Saito, H.; Yuasa, S.; Ando, K. Tunnel Magnetoresistance Effect in $Cr_{1-\delta}Te$/AlAs/ $Ga_{1-x}Mn_xAs$ Magnetic Tunnel Junctions. *J. Appl. Phys.* **2005**, *97*, 10D305.
4. Dijkstra, J.; Weitering, H. H.; van Bruggen, C. F.; Hass, C.; de Groot, R. A. Band-Structure Calculations, and Magnetic and Transport Properties of Ferromagnetic Chromium Tellurides (CrTe, Cr_3Te_4 and Cr_2Te_3). *J. Phys.: Condens. Matter* **1989**, *1*, 9141–9161.
5. Youn, S. J.; Kwon, S. K.; Min, B. I. Correlation Effect and Magnetic Moments in Cr_2Te_3. *J. Appl. Phys.* **2007**, *101*, 09G522.
6. Andresen, A. F. A Neutron Diffraction Investigation of Cr_2Te_3 and Cr_5Te_6. *Acta Chem. Scand.* **1963**, *17*, 1335–1342.
7. Andresen, A. F. The Magnetic Structure of Cr_2Te_3, Cr_3Te_4 and Cr_5Te_6. *Acta Chem. Scand.* **1970**, *24*, 3495–3509.
8. Hamasaki, T.; Hasimoto, T.; Yamaguchi, Y.; Watanabe, H. Neutron Diffraction Study of Cr_2Te_3 Single Crystal. *Solid State Commun.* **1975**, *16*, 895–897.
9. Kanomata, T.; Sugawara, Y.; Kamishima, K.; Mitamura, H.; Goto, T.; Ohta, S.; Kaneko, T. Pressure Effect on Spontaneous Magnetization of Cr_2Te_3 and Cr_5Te_6. *J. Magn. Magn. Matter* **1998**, *177−181*, 589–590.
10. Hashimoto, T.; Hoya, K.; Yamaguchi, M.; Ichitsubo, I. Magnetic Properties of Single Crystal $Cr_{2-\delta}Te_3$. *J. Phys. Soc. Jpn.* **1971**, *31*, 679–682.
11. Yuzuri, M.; Kanomata, T.; Kaneko, T. The Pressure Effect and the Curie Temperature and Exchange Striction of Cr_2S_3 and Cr_2Te_3. *J. Magn. Magn. Matter* **1987**, *70*, 223–224.
12. Hui, L.; Lim, S. T.; Bi, J. F.; Teo, K. L. Investigation on the Antiferromagnetic Component in the Intrinsic Exchange Bias in Structurally Single Phase Cr_2Te_3 Thin Film. *J. Appl. Phys.* **2012**, *111*, 07D719.
13. Sreenivasan, M. G.; Teo, X. J.; Jalil, M. B. A.; Liew, T.; Chong, T. C. Growth of CrTe Thin Films by Molecular Beam Epitaxy. *Thin Solid Films* **2006**, *505*, 133–136.
14. Sreenivasan, M. G.; Bi, J. F.; Teo, K. L.; Liew, T. Systematic Investigation of Structural and Magnetic Properties in Molecular Beam Epitaxial Growth of Metastable Zinc-Blende CrTe toward Half-Metallicity. *J. Appl. Phys.* **2008**, *103*, 043908.
15. Sreenivasan, M. G.; Teo, K. L.; Jalil, M. B. A.; Liew, T.; Chong, T. C.; Du, A. Y. Zinc-Blende Structure of CrTe Epilayers Grown on GaAs. *IEEE Trans. Magn.* **2006**, *42*, 2691.
16. McGuire, T. R.; Potter, R. I. Anisotropic Magnetoresistance in Ferromagnetic 3d Alloys. *IEEE Trans. Magn.* **1975**, *11*, 1018–1038.
17. Weller, D.; Moser, A.; Folks, L.; Best, M. E.; Lee, W.; Toney, M. F.; Schwickert, M.; Thiele, J.-U.; Doerner, M. F. High K_u Materials Approach to 100 Gbits/in^2. *IEEE Trans. Magn.* **2010**, *36*, 10.
18. Moser, A.; Takano, K.; Margulies, D. T.; Albrecht, M.; Sonobe, Y.; Ikeda, Y.; Sun, S.; Fullerton, E. E. Magnetic Recording: Advancing into the Future. *J. Phys. D: Appl. Phys.* **2002**, *35*, R157–R167.
19. Ikeda, S.; Miura, K.; Yamamoto, H.; Mizunuma, K.; Gan, H. D.; Endo, M.; Kanai, S.; Hayakawa, J.; Matsukura, F.; Ohno, H. A Perpendicular-Anisotropy CoFeB-MgO Magnetic Tunnel Junction. *Nat. Mater.* **2010**, *9*, 721–724.
20. Liu, L.; Pai, C.-F.; Li, Y.; Tseng, H. W.; Ralph, D. C.; Buhrman, R. A. Spin-Torque Switching with the Giant Spin Hall Effect of Tantalum. *Science* **2012**, *336*, 555–558.
21. Liu, L.; Lee, O. J.; Gudmundsen, T. J.; Ralph, D. C.; Buhrman, R. A. Current-Induced Switching of Perpendicularly Magnetized Magnetic Layers Using Spin Torque from the Spin Hall Effect. *Phys. Rev. Lett.* **2012**, *109*, 096602.
22. Roy, A.; Guchhait, S.; Sonde, S.; Dey, R.; Pramanik, T.; Rai, A.; Movva, H. C. P.; Colombo, L.; Banerjee, S. K. Two-Dimensional Weak Anti-Localization in Bi_2Te_3 Thin Film

Grown on Si(111)-(7×7) Surface by Molecular Beam Epitaxy. *Appl. Phys. Lett.* **2013**, *102*, 163118.
23. Shimada, K.; Saitoh, T.; Namatame, H.; Fujimori, A.; Ishida, S.; Asano, S.; Matoba, M.; Anzai, S. Photoemission Study of Itinerant Ferromagnet $Cr_{1-\delta}Te$. *Phys. Rev. B* **1996**, *53*, 7673.
24. Park, J.; Soh, Y.-A.; Aeppli, G.; Bland, S. R.; Zhu, X.-G.; Chen, X.; Xue, Q.-K.; Grey, F. Crystal Structure and Epitaxy of Bi_2Te_3 Films Grown on Si. *Appl. Phys. Lett.* **2012**, *101*, 221910.
25. He, L.; Xiu, F.; Wang, Y.; Fedorov, A. V.; Huang, G.; Kou, X.; Lang, M.; Beyermann, W. P.; Zou, J.; Wang, K. L. Epitaxial Growth of Bi_2Se_3 Topological Insulator Thin Films on Si(111). *J. Appl. Phys.* **2011**, *109*, 103702.
26. Li, H. D.; Wang, Z. Y.; Kan, X.; Guo, X.; He, H. T.; Wang, Z.; Wang, J. N.; Wong, T. L.; Wang, N.; Xie, M. H. The Van der Waals Epitaxy of Bi_2Se_3 on the Vicinal Si(111) Surface: An Approach for Preparing High-Quality Thin Films of a Topological Insulator. *New J. Phys.* **2010**, *12*, 103038.
27. Michely, T.; Hohage, M.; Bott, M.; Comsa, G. Inversion of Growth Speed Anisotropy in Two Dimensions. *Phys. Rev. Lett.* **1993**, *70*, 3943–3946.
28. Liu, S.; Zhang, Z.; Comsa, G.; Metiu, H. Kinetic Mechanism for Island Shape Variations Caused by Changes in the Growth Temperature. *Phys. Rev. Lett.* **1993**, *71*, 2967–2970.
29. Mahato, J. C.; Das, D.; Batabyal, R.; Roy, A.; Dev, B. N. Self-Organized Trench-Island Structures in Epitaxial Cobalt Silicide Growth on Si(111). *Surf. Sci.* **2014**, *620*, 23–29.
30. Cui, Y.; Li, L. Evolution of Spirals during Molecular Beam Epitaxy of GaN on 6H-SiC(0001). *Phys. Rev. B* **2002**, *66*, 155330.
31. Burton, W. K.; Cabrera, N.; Frank, F. C. The Growth of Crystals and the Equilibrium Structure of their Surfaces. *Philos. Trans. R. Soc. London A* **1951**, *243*, 299–358.
32. Duan, F.; Guojun, J. *Introduction to Condensed Matter Physics*; World Scientific Publishing Co. Pte. Ltd.: Singapore, 2005; Vol. 1.
33. Kamalakar, M. V.; Raychaudhuri, A. K. Low Temperature Electrical Transport in Ferromagnetic Ni Nanowires. *Phys. Rev. B* **2009**, *79*, 205417.
34. White, G. K.; Woods, S. B. Electrical and Thermal Resistivity of the Transition Elements at Low Temperatures. *Philos. Trans. R. Soc. London A* **1959**, *251*, 273–302.
35. Ferrer, D. A.; Guchhait, S.; Liu, H.; Ferdousi, F.; Corbet, C.; Xu, H.; Doczy, M.; Bourianoff, G.; Mathew, L.; Rao, R.; *et al.* Origin of Shape Anisotropy Effects in Solution-Phase Synthesized FePt Nanomagnets. *J. Appl. Phys.* **2011**, *110*, 014316.
36. Li, Y. B.; Zhang, Y. Q.; Li, W. F.; Li, D.; Li, J.; Zhang, Z. D. Spin-Glass-Like Behavior and Electrical Transport Properties of $Cr_7(Se_{1-x}Te_x)_8$. *Phys. Rev. B* **2006**, *73*, 212403.
37. Imry, Y.; Ma, S.-K. Random-Field Instability of the Ordered State of Continuous Symmetry. *Phys. Rev. Lett.* **1975**, *35*, 1399–1401.
38. Guchhait, S.; Jamil, M.; Ohldag, H.; Mehta, A.; Arenholz, E.; Lian, G.; LiFatou, A.; Ferrer, D. A.; Markert, J. T.; Colombo, L.; *et al.* Ferromagnetism in Mn-Implanted Epitaxially Grown Ge on Si(100). *Phys. Rev. B* **2011**, *84*, 024432.
39. Nam, D. N.; Jonason, K.; Nordblad, P.; Khiem, N. V.; Phuc, N. X. Coexistence of Ferromagnetic and Glassy Behavior in the $La_{0.5}Sr_{0.5}CoO_3$ Perovskite Compound. *Phys. Rev. B* **1999**, *59*, 4189–4194.
40. Mukherjee, S.; Ranganathan, R.; Anilkumar, P. S.; Roy, P. A. Static and Dynamic Response of Cluster Glass in $La_{0.5}Sr_{0.5}CoO_3$. *Phys. Rev. B* **1996**, *54*, 9267–9274.
41. Li, X.-G.; Fan, X. J.; Li, G.; Wu, W. B.; Wong, K. H.; Choy, C. L.; Ku, H. C. Field-Induced Crossover from Cluster-Glass to Ferromagnetic State in $La_{0.7}Sr_{0.3}Mn_{0.7}Co_{0.3}O_3$. *J. Appl. Phys.* **1999**, *85*, 1663–1666.
42. Matsukura, F.; Sawicki, M.; Dietl, T.; Chiba, D.; Ohno, H. Magnetotransport Properties of Metallic (Ga, Mn)As Films with Compressive and Tensile Strain. *Phys. E (Amsterdam, Neth.)* **2004**, *21*, 1032–1036.
43. Komori, F.; Kobayashi, S.; Sasaki, W. Electron Localization and Interaction in Two-Dimensional Magnetic Films. *J. Magn. Magn. Matter* **1983**, *35*, 74–76.
44. Wang, K. Y.; Edmonds, K. W.; Campion, R. P.; Zhao, L. X.; Foxon, C. T.; Gallagher, B. L. Anisotropic Magnetoresistance and Magnetic Anisotropy in High-Quality (Ga, Mn)As Films. *Phys. Rev. B* **2005**, *72*, 085201.
45. Chen, Y. J.; Lottis, D. K.; Dahlberg, E. D.; Kuznia, J. N.; Wowchak, A. M.; Cohen, P. I. Exchange Effects in Molecular-Beam-Epitaxy Grown Iron Films. *J. Appl. Phys.* **1991**, *69*, 4523–4525.
46. Sbiaa, R.; Meng, H.; Piramanayagam, S. N. Materials with Perpendicular Magnetic Anisotropy for Magnetic Random Access Memory. *Phys. Status Solidi RRL* **2011**, *5*, 413–419.
47. Mangin, S.; Ravelosona, D.; Katine, J. A.; Carey, M. J.; Terris, B. D.; Fullerton, E. E. Current-Induced Magnetization Reversal in Nanopillars with Perpendicular Anisotropy. *Nat. Mater.* **2006**, *5*, 210–215.
48. Roy, A.; Bhattacharjee, K.; Dev, B. N. Growth of $(\sqrt{3}\times\sqrt{3})$-Ag and (111) Oriented Ag Islands on Ge/Si(111) Surfaces. *Appl. Surf. Sci.* **2009**, *256*, 508–512.